ACS APPLIED NANO MATERIALS

www.acsanm.org Article

Controlling Quantum Confinement in Luminescent Perovskite Nanoparticles for Optoelectronic Devices by the Addition of Water

Anna Jancik Prochazkova, Yolanda Salinas, Cigdem Yumusak, Markus Clark Scharber, Oliver Brüggemann, Martin Weiter, Niyazi Serdar Sariciftci, Jozef Krajcovic, and Alexander Kovalenko*

Cite This: *ACS Appl. Nano Mater.* 2020, 3, 1242−1249 Read Online

ACCESS | Metrics & More | Article Recommendations | Supporting Information

ABSTRACT: Here, a simple method for controlling the size of the perovskite nanoparticles (PNPs) during preparation is reported. Metal halide PNPs have great potential for application in optoelectronic devices, such as light-emitting diodes, lasers, photodetectors, etc. They have exceptionally high photoluminescence quantum yields (PLQYs) and exhibit chemical tunability for versatile modifications of the perovskite structural composition, enabling the synthesis of nanoparticles with controlled size, shape, and optical properties. In this work, methylammonium lead bromide PNPs were prepared using a hygroscopic stabilizing ligand, tert-butoxycarbonyl-Lysine (tboc-Lysine). Water was used as an additive in the precursor solution, which resulted in the formation of highly mobile species and, thus, the nhancement of perovskite lattice growth. This method allowed the preparation of PNPs with controlled size between 4 and 7 nm. The quantum confinement effect led to a fine-tuned optical band gap of the nanoparticles. Increasing the amount of water added from 0 to 32 mol equiv with respect to Lead(II) bromide ($PbBr_2$) increased the PLQY to 70% in colloidal solutions and to 87% in thin films. Therefore, because of control over the size and high luminescent yields, the above-mentioned nanoparticles are targeted for use in optoelectronic devices.

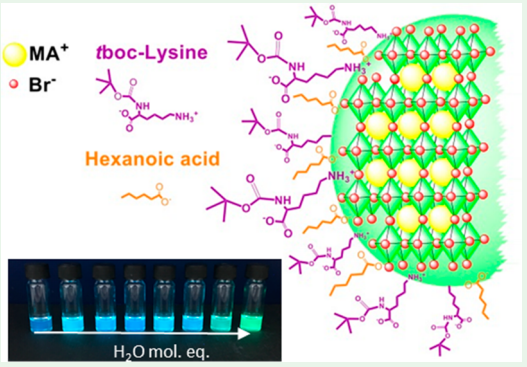

KEYWORDS: *perovskite nanoparticles, quantum confinement, size control, addition of water, ligands, amino acids, luminescence*

INTRODUCTION

Lead halide perovskite nanostructural materials have emerged in many forms, including inter alia spherical nanoparticles,[1] nanoplatelets,[2] nanorods,[3] and nanowires.[4] Particular attention has been focused on the extraordinary photoluminescence quantum yields (PLQYs), ranging up to 100%, of perovskite nanoparticles (PNPs), recently reported by Gonzalez-Carrero et al.[5] where the authors claimed the promising features of charge confinement and low defect concentration, demonstrating the possibility of lower sizes of perovskites in the nanoscale. Because of the quantum confinement effect,[6] the band gap of the individual particles increases compared to that of the bulk perovskite lattices. Given the band-gap tunability and exceptional luminescent properties of the perovskite nanostructural materials, there is no doubt about their application potential. PNPs can be used in optoelectronic devices, for example, photovoltaics,[7] photodetectors,[8] or light-emitting diodes (LEDs).[9]

Considering the processing aspect, one of the possibilities is to confine the size of PNPs during growth, dimensionally, by placing the precursors in a porous matrix, where the size of the pores defines the size of the crystallites.[10] However, this method places certain limitations on the porous substrates where PNPs are synthesized. On the other hand, colloidal techniques include hot injection,[11] ball milling,[12] nanocrystalline capping,[13] emulsion synthesis,[14] ligand-assisted precipitation,[5] a method where lead iodide (PbI_2) nanocrystals were used as templates,[15] and the recently reported diblock copolymer micelle templating method,[16] which resulted in control over the size distribution due to controlled nucleation and crystal growth. By following the aforementioned methods, a stable colloidal solution can be obtained and further deposited onto the desired substrate by various coating techniques such as spin coating,[17] centrifugal casting,[5] or inkjet printing.[18] It must be noted that the tunability of the band gap in all of the above-mentioned techniques was achieved by either alternating the lattice chemistry of the perovskite,[19] fitting the size of the precursor template nanocrystals,[15] or fine-tuning the ratio of capping agents.[13] In the present paper, we introduce a simple, yet elegant method for fine-tuning the PNP size and thus PNP optical properties by means of adding water.

Water is a significant consideration in perovskite-based devices because it decomposes the chemical structure, thus

Received: October 14, 2019
Accepted: January 7, 2020
Published: January 7, 2020

https://dx.doi.org/10.1021/acsanm.9b01857
ACS Appl. Nano Mater. 2020, 3, 1242−1249

making perovskite devices moisture-sensitive.[20] On the other hand, the addition of water helps to crystallize the perovskite lattice. Moreover, the presence of an optimal amount of water can solubilize the precursors in the solvent, providing them with higher mobility. This results in "healing" of the perovskite structure and removal of the excessive alkylammonium salt in the solution, thus reducing the amount of traps in the perovskite films.[21,22] It has been demonstrated[23] that anhydrous solvents used for perovskite-layer synthesis for solar cells, in fact, result in lower power conversion efficiencies. In this case, water weakly binds to the methylammonium molecules and forms a reversible hydrated phase within the perovskite, which quickly forms dehydrated perovskite after the thin-film deposition procedure. Additionally, interesting work reported by Hsieh and coauthors describes the preparation of perovskite thin films using an aqueous lead nitrate precursor.[24]

Taking these facts into consideration, it can be stated that water plays a crucial role in perovskite lattice crystallization.[25−29] This report focuses on the effect of the addition of water in the formation of thin perovskite films, which can be used primarily in solar cells[30−33] and photodetectors,[34−36] when the influence of water in the formation of perovskite nanostructures remains unreported. Therefore, in the present study, from a different point of view, we report a desirable function of water, which allows controllable quantum confinement in PNPs. The size of the PNP prepared by the ligand-assisted precipitation method[5] can be fine-tuned by the addition of a certain amount of water, and because of the formation size of the nanoparticles, the optical spectrum can be well-controlled as well. The key point in the present study is an implementation of *t*boc-Lysine surface ligands. It has been recently reported that *t*boc-Lysine can efficiently stabilize the methylammonium lead bromide perovskite surface during the formation of nanoparticles in the antisolvent medium.[37] Here, we show how, by means of the simple addition of water, it is possible to change the size and optical spectra of PNP stabilized by *t*boc-Lysine surface ligands.

RESULTS AND DISCUSSION

PNPs were prepared by a ligand-assisted precipitation method[5] (see Scheme 1). The emission maximum of the PNPs prepared

Scheme 1. Synthesis of the PNPs

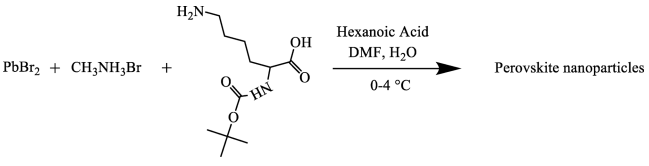

changed rapidly after the addition of water from 0 to 4 mol equiv, with an observed blue shift of up to 10 nm. The emission maximum changes are shown in Figure 1E, where the error bars came from a comparison of different batches; however, the trends in the individual batches were always the same. As a reference, a sample not containing water was used and exhibited a bright greenish-blue emission with an emission maximum at ∼490 nm. Interestingly, when the water addition was higher than >4 mol equiv with respect to $PbBr_2$, the emission maximum shifted to higher wavelengths (see Figure 1A), showing a direct correlation of the PNP features with the amount of water added to the precursor solution. It must be emphasized that the reference sample (0 mol equiv of water added) was not representative because the precursors were not completely dissolved even after 7 days of stirring, whereas a cloudy solution was formed. However, when a small amount of water (e.g., 0.4 mol equiv) was added, a more homogeneous solution was obtained, where all of the reagents were completely dissolved. In general, increasing amounts of water remarkably enhanced the PLQYs of the PNPs. In this context, the perovskite nanocrystals prepared without any water added exhibited a PLQY of 60%, but when 32 mol equiv of water with respect to $PbBr_2$ was added, the PLQY was further increased up to 70% (see Figure 1F). A similar increase of the PLQY in the solid state was also detected. Thin films prepared from PNPs without any water added exhibited a PLQY of 80%, and after the addition of water (32 mol equiv with respect to $PbBr_2$), the PLQY in the solid state increased in the range of 87−92.5%. In order to test the maximal PLQY enhancement to be achieved by this method, a sample containing double the amount of water (64 mol equiv with respect to $PbBr_2$) was prepared. In this case, an emission maximum of 508 nm in thin films and a PLQY of 5% were obtained, demonstrating the limit content of water needed to improve the PNP properties.

In order to investigate the origin of the shift in the emission spectra, transmission electron microscopy (TEM) used to determine the size of the samples. From the aforementioned experiment, it can be observed (see Figure 1H,I), that the PNP samples in which no water was added show significantly smaller nanoparticles at 4.6 ± 0.2 nm in comparison to the sample where 32 mol equiv of water was added; here, the average size of the PNPs was 6.2 ± 0.2 nm. The sample with 2.0 mol equiv of water addition contained PNPs with an average size of 4.0 ± 0.2 nm. Considering that the exciton Bohr radius for $MAPbBr_3$ is between 2.2 and 3.5 nm,[38] a band-gap broadening, and therefore a blue shift, can be fully associated with the quantum confinement effect: when the size of PNPs is smaller than 5−7 nm, the exciton is confined in the dimension, thus resulting in a size-dependent band gap. Overall, to determine the nanoparticle size, the images were taken from different positions in the sample, and we calculated the average size with the standard deviation. The mean size was calculated from 10 to 15 nanoparticles.

The optical stabilities of all colloidal solutions and thin films were tested. The PL spectra and PLQYs were measured after 2 days for samples with 0, 2.0, and 32 mol equiv of water with respect to $PbBr_2$ (see Figure S1). In general, after a certain aging time, both colloidal solutions and films exhibited shifting of the emission maxima to higher wavelengths. Interestingly, samples with no water added showed that the emission maxima shifted about 11 and 16 nm to higher wavelengths for films and colloidal solutions, respectively. On the contrary, samples with 32 mol equiv of water with respect to $PbBr_2$ possessed improved colloidal stability and red-shift wavelengths of 1 and 4 nm for films and colloidal solutions, respectively. Regarding spectral broadening, it was assumed that aggregates of nanoparticles were formed. Simultaneously, PLQY values were observed to decrease with time (see Figure S1). Notably, the sample with the most water added changed the least simply because it had the biggest nanoparticles, so a further increase in the size did not lead to changes in the quantum confinement insofar as the particle radius was bigger than the exciton radius.[38] The optical parameters of the colloidal solutions are summarized in Table 1.

Water-soluble amino acids usually show poor solubility in most organic solvents, including *N*,*N*-dimethylformamide

https://dx.doi.org/10.1021/acsanm.9b01857
ACS Appl. Nano Mater. 2020, 3, 1242−1249

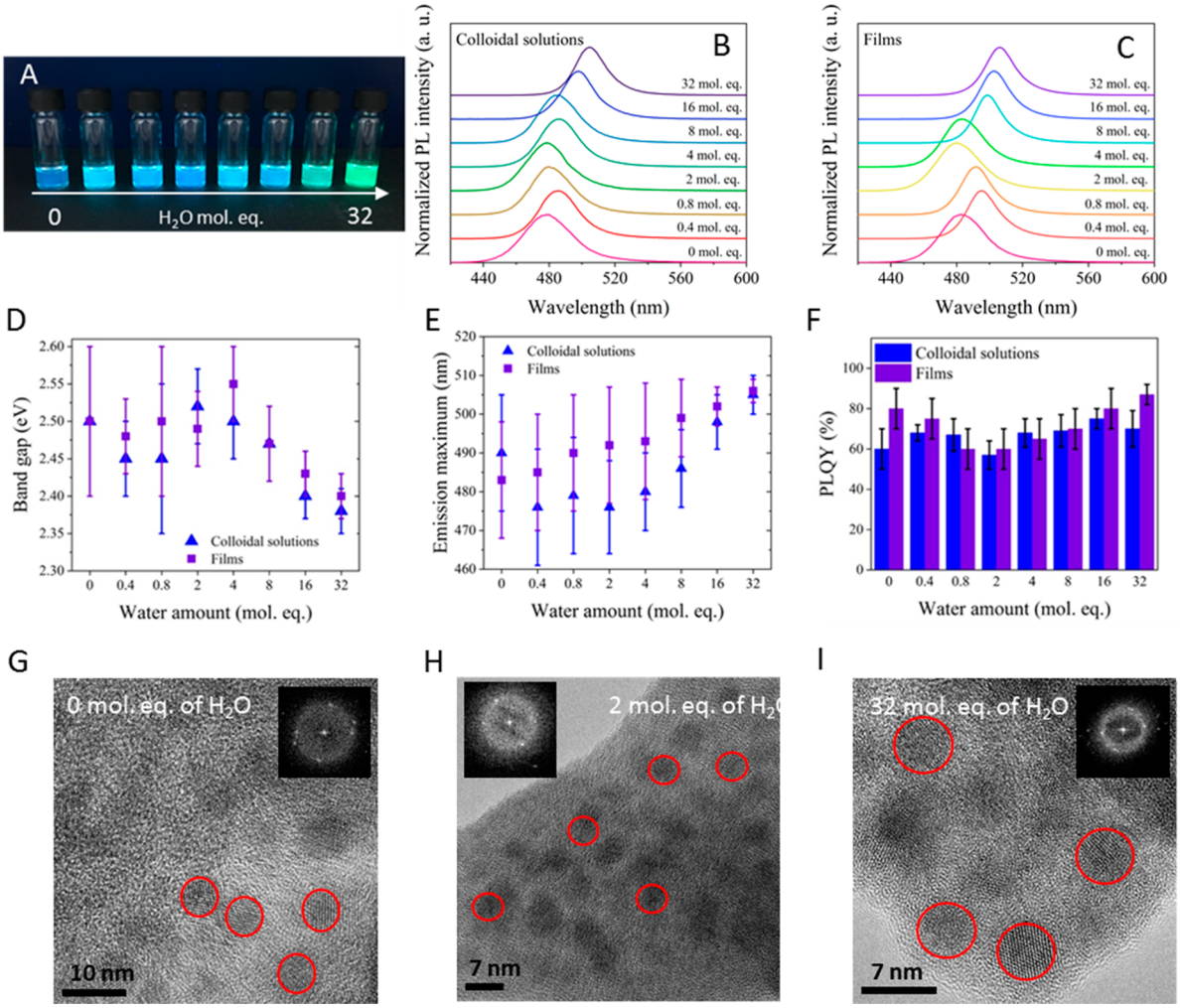

Figure 1. (A) Photograph of colloidal solutions prepared from precursor solutions with increasing amounts of water under ultraviolet (UV) irradiation (from left to right −0, 0.4, 0.8, 2.0, 4.0, 8.0, 16.0, and 32.0 mol equiv of water). (B) Normalized PL spectra of colloidal solutions. (C) Normalized PL spectra of thin films. (D) Band gaps calculated from Ultraviolet-Visible (UV−vis) spectra for colloidal solutions and films. (E) Emission maxima dependence on the water amount in precursor solutions, comparing colloidal solutions and thin films, (F) PLQYs of colloidal solutions and thin films with varying amounts of water. (G−I) TEM images with fast Fourier transform images (insets) of PNPs prepared with 0, 2, and 32 mol equiv of water, respectively.

Table 1. Optical Parameters of the Colloidal Solutions with Varying Amounts of Water Added

	band gap (eV)		emission maximum (nm)		full width at half-maximum (nm)		PLQY (%)	
mol equiv of water	solution	film	solution	film	solution	film	solution	film
0	2.50 ± 0.10	2.50 ± 0.10	490 ± 15	483 ± 15	34.25	31.57	60 ± 10	80 ± 10
0.4	2.45 ± 0.05	2.48 ± 0.05	476 ± 15	485 ± 15	28.00	23.06	68 ± 4	75 ± 10
0.8	2.45 ± 0.10	2.50 ± 0.10	479 ± 15	490 ± 15	29.80	31.92	67 ± 8	60 ± 10
2	2.52 ± 0.05	2.50 ± 0.05	476 ± 12	492 ± 15	29.80	22.92	57 ± 7	60 ± 10
4	2.50 ± 0.05	2.55 ± 0.05	480 ± 10	493 ± 15	28.19	29.05	68 ± 7	65 ± 10
8	2.47 ± 0.05	2.47 ± 0.05	486 ± 10	499 ± 10	29.14	20.29	69 ± 8	70 ± 10
16	2.40 ± 0.03	2.43 ± 0.03	498 ± 7	502 ± 5	23.56	22.07	75 ± 5	80 ± 10
32	2.38 ± 0.03	2.40 ± 0.03	505 ± 5	506 ± 3	22.20	21.80	70 ± 9	87 ± 5

(DMF),[39] as used in the present work. However, precursor solutions were slightly acidic in pH (ca. pH 6) because of possible protonation of the lysine amino group. In fact, protonated ammonium salts are known to be extremely hygroscopic;[40] thus, water molecules may mobilize ammonium salts within the precursor solution. Weak bonds between water molecules and ammonium groups of *t*boc-Lysine are formed in the solution; therefore, when precipitation occurs in the antisolvent medium, more mobile water-containing species are able to be formed and, hence, more effective nanocrystal formation occurs, resulting in smaller particle sizes. To support the aforementioned assumption, the theoretical investigation of molecular interactions was studied. The assumption of a difference in the PNP formation derives from the nature of the

https://dx.doi.org/10.1021/acsanm.9b01857
ACS Appl. Nano Mater. 2020, 3, 1242−1249

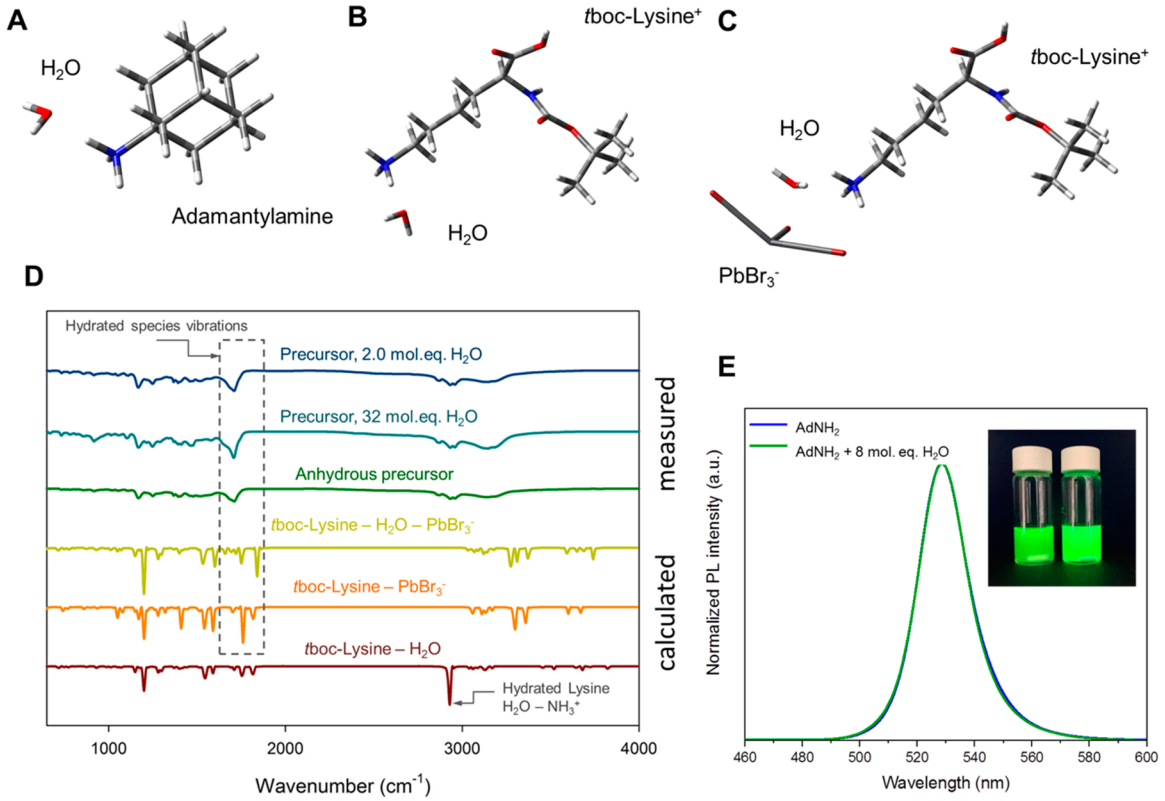

Figure 2. (A–C) B3LYP/6 311+G*-optimized geometries of the precursor complexes. (D) FTIR spectra show typical absorption peaks that are attributed to the presence of *t*boc-Lysine on the surfaces of nanoparticles. (E) PNP prepared using adamantylamine as the stabilizing ligand. No detectable changes in the emission maximum were observed.

intermediate phases that formed in the precursor solution, resulting from coordinative bonding.[41] Thus, various complex species in the precursor solution affect the nucleation and growth of the PNPs. In this regard, the complex adduct bonding nature was investigated using Fourier transform infrared (FTIR) spectroscopy[42] and supported by density quantum-chemical calculation.

To elucidate the mechanism of the influence of water on PNP formation, low-degree-of-complexity models were simulated using quantum-chemical calculations in order to predict the preferential generation of species under the effect of the solvent. Mainly geometry optimization and vibrational analysis were studied in order to gain deeper insight into the formation of coordination complexes in the precursor solution, which is a key locus for the formation of nanoparticles.

First of all, to compare adamantylamine with *t*boc-Lysine, we modeled the hydrated complexes of both compounds. By comparing the optimized geometry of both complexes modeled with the influence of the solvation medium, we find that indeed, in the case of the adamantylamine$^+$–H_2O complex, the distance between the water molecule and ammonium group is larger than that of *t*boc-Lysine$^+$–H_2O (1.75 vs 1.70 Å), and thus *t*boc-Lysine$^+$ forms a hydrate that is more stable than the one formed by adamantylamine.

Therefore, three types of coordination complexes were investigated: (a) *t*boc-Lysine$^+$–H_2O (see Figure 2B), (b) $PbBr_3$–*t*boc-Lysine$^+$, and (c) $PbBr_3$–*t*boc-Lysine$^+$–H_2O (see Figure 2A). Vibrational analysis from quantum-chemical modeling of part a showed a characteristic peak at ∼2800 cm^{-1} attributed to the hydrogen bond between water and *t*boc-Lysine$^+$. However, we assume that in the precursor this complex is not present; instead, the hydrated coordination complex of $PbBr_3$–*t*boc-Lysine$^+$–H_2O is a key structure in the formation of PNPs, where hydrated species showed vibration in a region of ∼1680 cm^{-1}. As can be observed from the FTIR spectra of the precursor solution containing varying amounts of water, the peak in that region clearly sharpens, but it still can be observed in the anhydrous solution insofar as partial hydration is possible during the measurements.

A comparison of the above-mentioned simulated results with FTIR spectroscopy (Figure 2D) of anhydrous and hydrated precursor solutions reveals a notable difference in the range of 1600–1700 cm^{-1}. Taking all of these facts into consideration, we can conclude that $PbBr_3^+$–*t*boc-Lysine$^-$ is indeed formed in the precursor solution. Considering that the water molecule is weakly bonded to the complex—the bond order was calculated as 0.14—the water molecule in the present case plays a significant role in PNP formation, in a manner in which the hydrated species are more mobile, but during the PNP formation, water molecules can be efficiently removed in the antisolvent medium.[43,44]

Moreover, taking into account the hygroscopic nature of the protonated amino acid used in the PNP preparation, water molecules could be bonded directly to the ammonium group of *t*boc-Lysine$^-$, confirming a dramatic increase in the solubility of *t*boc-Lysine in DMF when water was added. Nevertheless, on the FTIR spectrum, this region was overlapped by the $-CH_2$ vibrations.

Interestingly, if PNP were precipitated from the precursor solution containing adamantyl-1-amine, instead of the amino acid, as was previously described in the literature,[5] no detectable shift in the emission was observed (Figure 2D).

https://dx.doi.org/10.1021/acsanm.9b01857
ACS Appl. Nano Mater. 2020, 3, 1242–1249

Insofar as the water molecule can be coordinated to the $PbBr_3^+$ in both cases, most likely, the main characteristic affecting PNP formation by the addition of water is the hygroscopicity of the protonated *t*boc-Lysine$^-$; thus, mobilization of the ligands by the water molecule results in more efficient perovskite surface coverage and thus smaller PNPs.

Additionally, a dependence of the emission maxima was also observed in the solid-state samples. Thin films prepared by centrifugal casting onto glass substrates showed the same trend, where the optical shift increased with the amount of water added to the precursor solution. This indicates that the surfaces of the PNPs are stabilized, and thus they do not aggregate in the solid state.

Taking the above into account, it can be assumed that a low amount of water added increased the solubility of the precursors in the solution by the formation of mobile species weakly bonded to water molecules. Assumingly, because of the high hygroscopicity of the amino acid precursor, when the amount of water is relatively low, water molecules are mainly bonded to *t*boc-Lysine; thus, stabilization of the PNPs is more efficient. This results in a blue-shifted emission and an overall smaller size of the PNPs. However, with an increased amount of water added, further precursor complexes can be hydrated. Thus, water molecules are known to "heal" the perovskite lattice, and additional hydration of the precursor solution results in larger crystallites possessing remarkably high PLQYs. The presence of water, in this case, may reduce the concentration of lattice defects, which may act as traps.

It has to be noted that changes in the spectrum can be unlikely associated with hydration of the perovskite structure of the nanoparticles, insofar as hydration of the perovskite lattice would cause irreversible degradation of lead halide;[44,45] however, some amount of water reduces the surface and/or interfacial defects of the PNPs.[46] Thus, PLQYs can be observed when some amount of water is added to the precursor; however, this cannot be considered as hydration, insofar as hydrated perovskite has a much larger band gap of >3 eV and is not luminescent.[47]

Previous research on thin films showed that the addition of water results in larger crystallites in thin films.[48,49] Thus, in the present case, the mechanism is similar; however, the particles are confined by the surface ligands. Hygroscopicity of the surface ligands allows interaction between the ligands and water molecules in the precursor, thus affecting the formation of PNPs.

In general, the current approach displays fundamental findings on how the addition of water affects the physical and, therefore, the optical properties of methylammonium lead bromide PNPs stabilized by *t*boc-Lysine ligands. So far the biggest obstacle is providing ideally controlled conditions in the laboratory to provide a precise investigation with respect to the amount of water in the precursor solution, inasmuch as many factors have to be considered including the influence of ambient humidity during manipulation of the materials, poor control, or/and possible contamination of commercial products/gloveboxes. However, one can assume that, in a well-controlled industrial environment, it would be possible to implement such a method with a high level of precision.

CONCLUSION

In the present work, a simple nontemplate method of controlling the PNP size is described. Similar to the thin films, where the addition of water results in larger crystallites, and thus improved performance of the solar cells, here we used water to improve the mobility of the hygroscopic precursor, thus resulting in more efficient formation of the nanoparticles. As a result, $MAPbBr_3$ PNPs stabilized with amino acids were prepared by a ligand-assisted precipitation method, where the amino acid *t*boc-Lysine was used as the capping agent alongside the stabilizer HeA. Interestingly, hygroscopic protonated *t*boc-Lysine$^-$ formed complexes with additional water molecules, thus inducing the formation of mobile complexes that act as efficient precursors for PNP formation. To reach crystal lattice equilibrium, water molecules were efficiently removed during PNP crystallization because of weak interaction with the precursors. Thus, this promising method allows control of the PNPs' sizes without changing the chemistry of the nanoparticle core. Moreover, because of the "healing" effect of water molecules in the perovskite lattice, the addition of water dramatically increases the PLQY of PNPs because of the lower concentration of the lattice defects, which can act as traps, resulting in nonradiative transitions. Because of the excellent luminescent quantum yields and controllable sizes of the nanoparticles, they can be applied, for instance, in LEDs.

EXPERIMENTAL SECTION

Chemicals. Lead(II) bromide ($PbBr_2$; 99.999%) was purchased from Sigma-Aldrich. Methylammonium bromide (MABr) was purchased from GreatCell. *t*boc-L-Lysine (97%) was purchased from Alfa Aesar. Hexanoic acid (HeA; 98%) was purchased from TCI. Adamantyl-1-amine was obtained from Provicso CS. Anhydrous *N*,*N*-dimethylformamide (DMF) was purchased from Sigma-Aldrich. Toluene of reagent grade (≥99.8%) was purchased from VWR and used as received.

General Methods. Ultraviolet−visible (UV−vis) and fluorescence spectroscopies were used to characterize the optical properties of PNPs. UV−vis spectroscopy was carried out with a Lambda 1050 UV−vis−near-IR spectrometer (PerkinElmer). Photoluminescence (PL) spectra were measured on a fluorimeter from Photon Technology International. UV−vis and PL spectra of colloidal PNP suspensions were measured in a 1 × 1 cm quartz cuvette. For optical characterization of the films, an excitation wavelength of 405 nm at a 50° angle was used. The PLQYs of the colloidal PNP suspension and thin films were measured using an integrating-sphere Hamamatsu Photonics A9924-06, with a Shamrock SR-303i monochromator and an Andor iDus SiCCD detector at an excitation wavelength of 405 nm. Transmission electron microscopy (TEM) images were obtained with a Jeol JEM-2200 microscope using holey carbon film 300-mesh copper grids. All sample grids were previously treated for 5 min in a Jeol EC-52000IC ion cleaner before the TEM measurement. Fourier transform infrared spectroscopy (FTIR) spectra of precursor solutions were recorded on a PerkinElmer Spectrum 100. The precursor solutions were measured using an attenuated-total-reflectance technique under ambient conditions.

X-ray Photoelectron Spectroscopy (XPS). XPS was measured in order to provide the binding energy of a core-level electron of an atom in the nanoparticles.[50] The binding energy, in turn, strongly depends on the chemical environment of the atom and therefore is used to determine the chemical bonding of the material. XPS sputter depth profiles were performed using a Thetaprobe XPS system (Thermo Scientific, U.K.), which was controlled and operated by the *Avantage* software package from the system manufacturer. The device was equipped with a monochromated Al Kα X-ray source ($h\nu$ = 1486.6 eV) and a dual flood gun for neutralizing the surface charges. The X-ray spot on the sample surface exhibited a diameter of 400 μm. Sputtering was performed by using a Ar^+-ion gun. The survey spectra were recorded with 200 eV of pass energy and with a binding energy step of 1 eV, while for high-resolution spectra, a pass energy of 20 eV and a step of 0.05 eV were taken. For the PNPs, the Pb 4f XPS spectra

https://dx.doi.org/10.1021/acsanm.9b01857
ACS Appl. Nano Mater. 2020, 3, 1242−1249

showed two characteristic symmetric peaks at 138.4 and 143.3 eV, attributed to Pb $4f_{7/2}$ and Pb $4f_{5/2}$, respectively. The spin−orbit splitting was 4.86 eV, which corresponds to the previously reported results.[51,52] The presence of metallic lead was confirmed with peaks at 136.4 and 141.3 eV, which could point to the lead(0)-rich surface of the nanoparticles.[53,54] On the Br 3d XPS spectrum, two peaks, at 68.2 and 69.2 eV, were observed, which correspond to Br $3d_{5/2}$ and Br $3d_{3/2}$, respectively.[53] The N 1s XPS spectrum was split into two peaks with centers at 400.0 and 401.8 eV; these peaks can be associated with the amide group[51] of *t*boc-Lysine and with the ammonium salts of the primary amine of *t*boc-Lysine[55] and of the methylammonium salt,[52] respectively. Additionally, the presence of only the peak at 401.8 eV points to the charged character of the primary ammonium group in the side chain of *t*boc-Lysine. The O 1s XPS spectrum exhibited peaks at 531.8 and 533.3 eV associated with the carboxylate species C═O and C−O, respectively. In the C 1s XPS spectrum, we observed four peaks: the peak at 285.0 eV can be assigned to C−C and C−H bonds, followed by another peak at 286.1 eV that can be attributed to the C−N bond of the amino group, the C−N bond of the amide group was proven by the peak at 287.1 eV, and, finally, the peak at the highest binding energy of 289.4 eV can be assigned to the C−O bond of the carboxylic acid group.[56] Because of the ionic form of the carboxylic acid, only the C−O bond was proven in the spectra because of delocalization of the negative charge among the carboxylic acid group.[57] (For the scan images, see the Supporting Information.)

Quantum-Chemical Calculations. For the quantum-chemical modeling, in order to calculate the bond lengths and orders and to visualize the molecular orbitals of the complexes, the *Gaussian 09* software package was applied. A Becke, three-parameter, Lee−Yang−Parr (B3LYP) functional expanded by 6-311+G* with split-valence-polarized triple-ζ basis set polarization and diffuse functions on heavy atoms for the C, N, H, and O atoms and Los Alamos National Laboratory 2 double-ζ (LANL2DZ) was used for heavy atoms. Force constants and the resulting vibrational frequencies were computed in order to simulate the IR spectra of the complexes.

Preparation of Colloidal Solutions of PNPs. Initially, the precursor solutions were prepared by mixing $PbBr_2$, MABr, HeA, and *t*boc-Lysine in anhydrous DMF, at concentrations of 0.027, 0.030, 0.258, and 0.22 mol L^{-1}, respectively, resulting in a final molar ratio of 1:1.1:9.5:0.8. Consequently, a certain amount of 18 MΩ ultrapure water was added to the precursor solutions in molar equivalents of water with respect to $PbBr_2$ of 0.0, 0.4, 0.8, 2.0, 4.0, 8.0, 16, 32, and 64. It must be noted that all of the solid perovskite precursor components were freeze-dried prior to dissolution. All of the manipulations were carried out in a glovebox under a nitrogen atmosphere unless otherwise stated. In order to enhance the solubility of the reagents and ensure complex formation, all of the precursor solutions were stirred in the glovebox for 7 days. After this time, the PNPs were precipitated from the glovebox by the addition of 20 μL of a precursor solution with toluene (10 mL), under cold conditions (0−4 °C). The resulting colloidal solutions were isolated by centrifugation and finally washed and redispersed in 10 mL of toluene. Directly after, the PNPs formed were redispersed in toluene, and thin films were prepared. For that, samples with 0.0, 0.4, 0.8, 2.0, 4.0, 8.0, 16, 32, and 64 mol equiv of water were used. Then, the colloidal solutions were centrifugally casted onto glass substrates (1 × 1 cm) at 5000 rpm for 10 min according to the approach reported by Gonzalez-Carrero et al.[5] Consequently, the films were dried under ambient conditions.

Interestingly, when freeze-dried chemicals were used for the precursor solutions' preparation, the sample with no addition of water was not fully dissolved. Thus, all of the precursor solutions were stirred in the glovebox for 7 days to provide the appropriate complexation. In all of the other cases, the presence of water significantly increased the solubility of *t*boc-Lysine in the precursor solution.

Preparation of Adamantyl-1-amine PNP Precursor Solutions. $PbBr_2$, MABr, HeA, and adamantyl-1-amine were mixed in anhydrous DMF at concentrations of 0.027, 0.030, 0.258, and 0.22 mol L^{-1}, respectively, resulting in a final molar ratio of 1:1.1:9.5:0.8. Simultaneously, two precursor solutions were prepared: one used as a control and another containing 8 mol equiv of water with respect to $PbBr_2$. The PNPs were prepared by precipitating 20 μL of the corresponding precursor solution in 10 mL of toluene in an ice bath (0−3 °C). For the film preparation, the precursor solution (50 μL) was precipitated in toluene (25 mL) in an ice bath with stirring at 1000 rpm. A glass substrate was placed in a centrifugation tube, and the PNPs were centrifugally casted onto the substrate at 5000 rpm for 12 min. The supernatant was discharged, and then the film was dried under ambient conditions.

■ ASSOCIATED CONTENT

Supporting Information

The Supporting Information is available free of charge at https://pubs.acs.org/doi/10.1021/acsanm.9b01857.

Stability of optical property colloidal solutions (Figure S1), TEM images of PNPs (Figures S2−S5), and XPS spectra of PNPs (Figure S5) (PDF)

■ AUTHOR INFORMATION

Corresponding Author

Alexander Kovalenko − *Johannes Kepler University Linz, Linz, Austria, and Brno University of Technology, Brno, Czech Republic;* orcid.org/0000-0002-7194-1874; Email: kovalenko.alx@gmail.com

Other Authors

Anna Jancik Prochazkova − *Johannes Kepler University Linz, Linz, Austria, and Brno University of Technology, Brno, Czech Republic*

Yolanda Salinas − *Johannes Kepler University Linz, Linz, Austria;* orcid.org/0000-0002-1828-5839

Cigdem Yumusak − *Johannes Kepler University Linz, Linz, Austria*

Markus Clark Scharber − *Johannes Kepler University Linz, Linz, Austria;* orcid.org/0000-0002-4918-4803

Oliver Brüggemann − *Johannes Kepler University Linz, Linz, Austria*

Martin Weiter − *Brno University of Technology, Brno, Czech Republic*

Niyazi Serdar Sariciftci − *Johannes Kepler University Linz, Linz, Austria*

Jozef Krajcovic − *Brno University of Technology, Brno, Czech Republic*

Complete contact information is available at: https://pubs.acs.org/10.1021/acsanm.9b01857

Notes

The authors declare no competing financial interest.

■ ACKNOWLEDGMENTS

The authors acknowledge support from the Operational Programme Research, Development and Education, European Regional Development Fund (Project CZ.02.1.01/0.0/0.0/16_019/0000754) of the Ministry of Education, Youth and Sports of the Czech Republic, from the Czech Science Foundation (Project 19-23718S), and from the Ministry of Industry and Trade TRIO (Project FV20022). We gratefully acknowledge financial support of the Austrian Science Fund FWF within the Wittgenstein Prize for N.S.S.

REFERENCES

(1) Schmidt, L. C.; Pertegas, A.; Gonzalez-Carrero, S.; Malinkiewicz, O.; Agouram, S.; MinguezEspallargas, G.; Bolink, H. J.; Galian, R. E.; Perez-Prieto, J. Nontemplate synthesis of $CH_3NH_3PbBr_3$ perovskite nanoparticles. *J. Am. Chem. Soc.* **2014**, *136*, 850−853.

(2) Weidman, M. C.; Goodman, A. J.; Tisdale, W. A. Colloidal Halide Perovskite Nanoplatelets: An Exciting New Class of Semiconductor Nanomaterials. *Chem. Mater.* **2017**, *29*, 5019−5030.

(3) Aharon, S.; Etgar, L. Two Dimensional Organometal Halide Perovskite Nanorods with Tunable Optical Properties. *Nano Lett.* **2016**, *16*, 3230−3235.

(4) Feng, J.; Gong, C.; Gao, H.; Wen, W.; Gong, Y.; Jiang, X.; Zhang, B.; Wu, Y.; Wu, Y.; Fu, H.; Jiang, L.; Zhang, X. Single-crystalline layered metal-halide perovskite nanowires for ultrasensitive photodetectors. *Nature Electronics.* **2018**, *1*, 404−410.

(5) Gonzalez-Carrero, S.; Martinez-Sarti, M.; Sessolo, M.; Galian, R. E.; Perez-Prieto, J. Highly photoluminescent, dense solid films from organic-capped $CH_3NH_3PbBr_3$ perovskite colloids. *J. Mater. Chem. C* **2018**, *6*, 6771−6777.

(6) Kumar, P.; Muthu, C.; Nair, V. C.; Narayan, K. S. Quantum Confinement Effects in Organic Lead Tribromide Perovskite Nanoparticles. *J. Phys. Chem. C* **2016**, *120*, 18333−18339.

(7) Gao, Y.; Wu, Y.; Lu, H.; Chen, C.; Liu, Y.; Bai, X.; Yang, L.; Yu, W. W.; Dai, Q.; Zhang, Y. $CsPbBr_3$ perovskite nanoparticles as additive for environmentally stable perovskite solar cells with 20.46% efficiency. *Nano Energy* **2019**, *59*, 517−526.

(8) Li, J.; Shen, Y.; Liu, Y.; Shi, F.; Ren, X.; Niu, T.; Zhao, K.; Liu, S. F. Stable High-Performance Flexible Photodetector Based on Upconversion Nanoparticles/Perovskite Microarrays Composite. *ACS Appl. Mater. Interfaces* **2017**, *9*, 19176−19183.

(9) Li, G.; Tan, Z.-K.; Di, D.; Lai, M. L.; Jiang, L.; Lim, J. H.-W.; Friend, R. H.; Greenham, N. C. Efficient Light-Emitting Diodes Based on Nanocrystalline Perovskite in a Dielectric Polymer Matrix. *Nano Lett.* **2015**, *15*, 2640−2644.

(10) Demchyshyn, S.; Roemer, J. M.; Groiß, H.; Heilbrunner, H.; Ulbricht, C.; Apaydin, D.; Böhm, A.; Rütt, U.; Bertram, F.; Hesser, G.; Scharber, M. C.; Sariciftci, N. S.; Nickel, B.; Bauer, S.; Głowacki, E. D.; Kaltenbrunner, M. Confining metal-halide perovskites in nanoporous thin films. *Science Advances* **2017**, *3*, No. e1700738.

(11) Lim, S.-C.; Lin, H.-P.; Tsai, W.-L.; Lin, H.-W.; Hsu, Y.-T.; Tuan, H.-Y. Binary halide, ternary perovskite-like, and perovskite-derivate nanostructures: hot injection synthesis and optical and photocatalytic properties. *Nanoscale* **2017**, *9*, 3747−3751.

(12) Protesescu, L.; Yakunin, S.; Nazarenko, O.; Dirin, D. N.; Kovalenko, M. V. Low-Cost Synthesis of Highly Luminescent Colloidal Lead Halide Perovskite Nanocrystals by Wet Ball Milling. *ACS Appl. Nano Mater.* **2018**, *1*, 1300−1308.

(13) Sichert, J. A.; Tong, Y.; Mutz, N.; Vollmer, M.; Fischer, S.; Milowska, K. Z.; García Cortadella, R.; Nickel, B.; Cardenas-Daw, C.; Stolarczyk, J. K.; Urban, A. S.; Feldmann, J. Quantum size effect in organometal halide perovskite nanoplatelets. *Nano Lett.* **2015**, *15*, 6521−6527.

(14) Huang, H.; Zhao, F.; Liu, L.; Zhang, F.; Wu, X. G.; Shi, L.; Zou, B.; Pei, Q.; Zhong, H. Emulsion synthesis of size-tunable $CH_3NH_3PbBr_3$ quantum dots: An alternative route toward efficient light-emitting diodes. *ACS Appl. Mater. Interfaces* **2015**, *7*, 28128−28133.

(15) Hassan, Y.; Song, Y.; Pensack, R. D.; Abdelrahman, A. I.; Kobayashi, Y.; Winnik, M. A.; Scholes, G. D. Structure-tuned lead halide perovskite nanocrystals. *Adv. Mater.* **2016**, *28*, 566−573.

(16) Hui, L. S.; Beswick, C.; Getachew, A.; Heilbrunner, H.; Liang, K.; Hanta, G.; Arbi, R.; Munir, M.; Dawood, H.; IsikGoktas, N.; LaPierre, R.; Scharber, M. C.; Sariciftci, N. S.; Turak, A. Reverse Micelle Templating Route to Ordered Monodispersed Spherical Organo-Lead Halide Perovskite Nanoparticles for Light Emission. *ACS Appl. Nano Mater.* **2019**, *2*, 4121−4132.

(17) Song, J.; Li, J.; Li, X.; Xu, L.; Dong, Y.; Zeng, H. Quantum Dot Light-Emitting Diodes Based on Inorganic Perovskite Cesium Lead Halides (CsPbX3). *Adv. Mater.* **2015**, *27*, 7162−7167.

(18) Ilie, C. C.; Guzman, F.; Swanson, B. L.; Evans, I. R.; Costa, P. S.; Teeter, J. D.; Shekhirev, M.; Benker, N.; Sikich, S.; Enders, A.; Dowben, P. A.; Sinitskii, A.; Yost, A. J. Inkjet printable-photoactive all inorganic perovskite films with long effective photocarrier lifetimes. *J. Phys.: Condens. Matter* **2018**, *30*, 18LT02.

(19) Sutton, R. J.; Eperon, G. E.; Miranda, L.; Parrott, E. S.; Kamino, B. A.; Patel, J. B.; Hörantner, M. T.; Johnston, M. B.; Haghighirad, A. A.; Moore, D. T.; Snaith, H. J. Bandgap-Tunable Cesium Lead Halide Perovskites with High Thermal Stability for Efficient Solar Cells. *Adv. Energy Mater.* **2016**, *6*, 1502458.

(20) Huang, J.; Tan, S.; Lund, P. D.; Zhou, H. Impact of H_2O on organic-inorganic hybrid perovskite solar cells. *Energy Environ. Sci.* **2017**, *10*, 2284−2311.

(21) Dubey, A.; Saini, P.; Qiao, Q. *Fundamentals of Conjugated Polymer Blends, Copolymers and Composites*; John Wiley & Sons, Inc., 2015; Chapter 5, pp 281−338.

(22) Chueh, C. C.; Liao, C.-Y.; Zuo, F.; Williams, S. T.; Liang, P. W.; Jen, A. K.-Y. The roles of alkyl halide additives in enhancing perovskite solar cell performance. *J. Mater. Chem. A* **2015**, *3*, 9058−9062.

(23) Liu, D.; Traverse, C. J.; Chen, P.; Elinski, M.; Yang, C.; Wang, L.; Young, M.; Lunt, R. R. Aqueous-Containing Precursor Solutions for Efficient Perovskite Solar Cells. *Adv. Sci.* **2018**, *5*, 1700484.

(24) Hsieh, T.-Y.; Wei, T.-C.; Wu, K.-L.; Ikegami, M.; Miyasaka, T. Efficient perovskite solar cells fabricated using an aqueous lead nitrate precursor. *Chem. Commun.* **2015**, *51*, 13294−13297.

(25) Zhang, W.; Xiong, J.; Li, J.; Daoud, W. A. Mechanism of Water Effect on Enhancing the Photovoltaic Performance of Triple-Cation Hybrid Perovskite Solar Cells. *ACS Appl. Mater. Interfaces* **2019**, *11*, 12699−12708.

(26) Gong, X.; Li, M.; Shi, X.-B.; Ma, H.; Wang, Z.-K.; Liao, L.-S. Controllable Perovskite Crystallization by Addition of water for High-Performance Solar Cells. *Adv. Funct. Mater.* **2015**, *25*, 6671−6678.

(27) Dubey, A. M. S. Study of Moisture and Water Effects in Low Temperature Crystallization of Perovskite Film for Efficient Solar Cells. Ph.D. Dissertation, South Dakota State University, Brookings, SD, 2016.

(28) Adhikari, N.; Dubey, A.; Gaml, E. A.; Vaagensmith, B.; Reza, K. M.; Mabrouk, S. A. A.; Gu, S.; Zai, J.; Qian, X.; Qiao, Q. Crystallization of a perovskite film for higher performance solar cells by controlling water concentration in methyl ammonium iodide precursor solution. *Nanoscale* **2016**, *8*, 2693−2703.

(29) Zhou, X.; Zhang, Y.; Kong, W.; Hu, M.; Zhang, L.; Liu, C.; Li, X.; Pan, C.; Yu, G.; Cheng, C.; Xu, B. Crystallization Manipulation and Morphology Evolution for Highly Efficient Perovskite Solar Cell Fabrication via Hydration Water Induced Intermediate Phase Formation under Heat Assisted Spin-Coating. *J. Mater. Chem. A* **2018**, *6*, 3012−3021.

(30) Zhang, W.; Xiong, J.; Li, J.; Daoud, W. A. Mechanism of Water Effect on Enhancing the Photovoltaic Performance of Triple-Cation Hybrid Perovskite Solar Cells. *ACS Appl. Mater. Interfaces* **2019**, *11*, 12699−12708.

(31) Gong, X.; Li, M.; Shi, X.-B.; Ma, H.; Wang, Z.-K.; Liao, L.-S. Controllable Perovskite Crystallization by Addition of water for High-Performance Solar Cells. *Adv. Funct. Mater.* **2015**, *25*, 6671−6678.

(32) Liu, D.; Traverse, C. J.; Chen, P.; Elinski, M.; Yang, C.; Wang, L.; Young, M.; Lunt, R. R. Aqueous-Containing Precursor Solutions for Efficient Perovskite Solar Cells. *Adv. Sci.* **2018**, *5*, 1700484.

(33) Wu, C.-G.; Chiang, C.-H.; Tseng, Z.-L.; Nazeeruddin, M. K.; Hagfeldt, A.; Grätzel, M. High efficiency stable inverted perovskite solar cells without current hysteresis. *Energy Environ. Sci.* **2015**, *8*, 2725−2733.

(34) Miao, J.; Zhang, F. Recent progress on highly sensitive perovskite photodetectors. *J. Mater. Chem. C* **2019**, *7*, 1741−1791.

(35) Zhang, M.; Zhang, F.; Wang, Y.; Zhu, L.; Hu, Y.; Lou, Z.; Hou, Y.; Teng, F. High-Performance Photodiode-Type Photodetectors Based on Polycrystalline Formamidinium Lead Iodide Perovskite Thin Films. *Sci. Rep.* **2018**, *8*, 11157.

https://dx.doi.org/10.1021/acsanm.9b01857
ACS Appl. Nano Mater. 2020, 3, 1242−1249

(36) Xue, J.; Zhu, Z.; Xu, X.; Gu, Y.; Wang, S.; Xu, L.; Zou, Y.; Song, J.; Zeng, H.; Chen, Q. Narrowband Perovskite Photodetector-Based Image Array for Potential Application in Artificial Vision. *Nano Lett.* **2018**, *18*, 7628−7634.
(37) JancikProchazkova, A.; Demchyshyn, S.; Yumusak, C.; MáSilko, J.; Brüggemann, O.; Weiter, M.; Kaltenbrunner, M.; Sariciftci, N. S.; Krajcovic, J.; Salinas, Y.; Kovalenko, A. Proteinogenic Amino Acid Assisted Preparation of Highly Luminescent Hybrid Perovskite Nanoparticles. *ACS Appl. Nano Mater.* **2019**, *2*, 4267−4274.
(38) Wang, Q.; Liu, X.-D.; Qiu, Y.-H.; Chen, K.; Zhou, L.; Wang, Q.-Q. Quantum confinement effect and exciton binding energy of layered perovskite nanoplatelets. *AIP Adv.* **2018**, *8*, 025108.
(39) Needham, T. E. The Solubility of Amino Acids in Various Solvent Systems. Ph.D. Dissertation, University of Rhode Island, Kingston, RI, 1970.
(40) Hu, D.; Chen, J.; Ye, X.; Li, L.; Yang, X. Hygroscopicity and evaporation of ammonium chloride and ammonium nitrate: Relative humidity and size effects on the growth factor. *Atmos. Environ.* **2011**, *45*, 2349−2355.
(41) Lee, J.-W.; Dai, Z.; Lee, C.; Lee, H. M.; Han, T.-H.; De Marco, N.; Lin, O.; Choi, C. S.; Dunn, B. S.; Koh, J.; Di Carlo, D.; Ko, J. H.; Maynard, H. D.; Yang, Y. Tuning Molecular Interactions for Highly Reproducible and Efficient Formamidinium Perovskite Solar Cells via Adduct Approach. *J. Am. Chem. Soc.* **2018**, *140*, 6317−6324.
(42) Hassan, Y.; Ashton, O. J.; Park, J. H.; Li, G.; Sakai, N.; Wenger, B.; Haghighirad, A. A.; Noel, N. K.; Song, M. H.; Lee, B. R.; Friend, R. H.; Snaith, H. J. Facile Synthesis of Stable and Highly Luminescent Methylammonium Lead Halide Nanocrystals for Efficient Light Emitting Devices. *J. Am. Chem. Soc.* **2019**, *141*, 1269−1279.
(43) Huang, J.; Tan, S.; Lund, P. D.; Zhou, H. Impact of H_2O on organic-inorganic hybrid perovskite solar cells. *Energy Environ. Sci.* **2017**, *10*, 2284−2311.
(44) Eperon, G. E.; Habisreutinger, S. N.; Leijtens, T.; Bruijnaers, B.; van Franeker, J. J.; deQuilettes, D. W.; Pathak, S.; Sutton, R. J.; Grancini, G.; Ginger, D. S.; Janssen, R. A. J.; Petrozza, A.; Snaith, H. J. The importance of Moisture in Hybrid Lead Halide Perovskite Thin Film Fabrication. *ACS Nano* **2015**, *9*, 9380−9393.
(45) Kye, Y.-H.; Yu, C.-J.; Jong, U.-G.; Chen, Y.; Walsh, A. Critical Role of Water in Defect Aggregation and Chemical Degradation of Perovskite Solar Cells. *J. Phys. Chem. Lett.* **2018**, *9*, 2196−2201.
(46) Howard, J. M.; Tennyson, E. M.; Barik, S.; Szostak, R.; Waks, E.; Toney, M. F.; Nogueira, A. F.; Neves, B. R. A.; Leite, M. S. Humidity-Induced Photoluminescence Hysteresis in Variable Cs/Br Ratio Hybrid Perovskites. *J. Phys. Chem. Lett.* **2018**, *9*, 3463−3469.
(47) Leguy, A. M. A.; Hu, Y.; Campoy-Quiles, M.; Alonso, M. I.; Weber, O. J.; Azarhoosh, P.; van Schilfgaarde, M.; Weller, M. T.; Bein, T.; Nelson, J.; Docampo, P.; Barnes, P. R. F. Reversible Hydration of $CH_3NH_3PbI_3$ in Films, Single Crystals, and Solar Cells. *Chem. Mater.* **2015**, *27*, 3397−3407.
(48) Pathak, S.; Sepe, A.; Sadhanala, A.; Deschler, F.; Haghighirad, A.; Sakai, N.; Goedel, K. C.; Stranks, S. D.; Noel, N.; Price, M.; Huttner, S.; Hawkins, N. A.; Friend, R. H.; Steiner, U.; Snaith, H. J. Atmospheric Influence upon Crystallization and Electronic Disorder and Its Impact on the Photophysical Properties of Organic-Inorganic Perovskite Solar Cells. *ACS Nano* **2015**, *9*, 2311−2320.
(49) Cheng, Y.; So, F.; Tsang, S.-W. Progress in air-processed perovskite solar cells: from crystallization to photovoltaic performance. *Mater. Horiz.* **2019**, *6*, 1611−1624.
(50) Greczynski, G.; Hultman, L. X-ray photoelectron spectroscopy: Towards reliable binding energy referencing. *Prog. Mater. Sci.* **2020**, *107*, 100591.
(51) Acik, M.; Park, I. K.; Koritala, R. E.; Lee, G.; Rosenberg, R. A. Oxygen-induced defects at the lead halide perovskite/graphene oxide interfaces. *J. Mater. Chem. A* **2018**, *6*, 1423−1442.
(52) Gonzalez-Carrero, S.; Galian, R. E.; Perez-Prieto, J. Maximizing the emissive properties of $CH_3NH_3PbBr_3$ perovskite nanoparticles. *J. Mater. Chem. A* **2015**, *3*, 9187−9193.
(53) Yi, N.; Wang, S.; Duan, Z.; Wang, K.; Song, Q.; Xiao, S. Tailoring the Performances of Lead Halide Perovskite Devices with Electron-Beam Irradiation. *Adv. Mater.* **2017**, *29*, 1701636.
(54) Ederer, J.; Janoš, P.; Ecorchard, P.; Tolasz, J.; Štengl, V.; Beneš, H.; Perchacz, M.; Pop-Georgievski, O. Determination of amino groups on functionalized graphene oxide for polyurethane nanomaterials: XPS quantitation vs. functional speciation. *RSC Adv.* **2017**, *7*, 12464−12473.
(55) Niedziałkowski, P.; Ossowski, T.; Zięba, P.; Cirocka, A.; Rochowski, P.; Pogorzelski, S. J.; Ryl, J.; Sobaszek, M.; Bogdanowicz, R. Poly-L-lysine-modified boron-doped diamond electrodes for the amperometric detection of nucleic acid bases. *J. Electroanal. Chem.* **2015**, *756*, 84−93.
(56) Lashkor, M.; Rawson, F. J.; Preece, J. A.; Mendes, P. M. Switching specific biomolecular interactions on surfaces under complex biological conditions. *Analyst* **2014**, *139*, 5400−5408.
(57) Wang, Y.; Li, L.; Dai, P.; Yan, L.; Cao, L.; Gu, X.; Zhao, X. Missing-node directed synthesis of hierarchical pores on a zirconium metal-organic framework with tunable porosity and enhanced surface acidity via a microdroplet flow reaction. *J. Mater. Chem. A* **2017**, *5*, 22372−22379.

https://dx.doi.org/10.1021/acsanm.9b01857
ACS Appl. Nano Mater. 2020, 3, 1242−1249